Astronomy
&
Astrophysics

X-ray/UV campaign on the Mrk 279 outflow: Density diagnostics in Active Galactic Nuclei using O v K-shell absorption lines

J. S. Kaastra[1], A. J. J. Raassen[1,2], R. Mewe[1,†*], N. Arav[3], E. Behar[4], E. Costantini[1], J. R. Gabel[3], G. A. Kriss[5], D. Proga[3], M. Sako[6], and K. C. Steenbrugge[1]

[1] SRON National Institute for Space Research Sorbonnelaan 2, 3584 CA Utrecht, The Netherlands
    e-mail: J.Kaastra@sron.nl
[2] Astronomical Institute "Anton Pannekoek", Kruislaan 403, 1098 SJ Amsterdam, The Netherlands
[3] CASA, University of Colorado, 389 UCB, Boulder, CO 80309-0389, USA
[4] Department of Physics, Technion-Israel Institute of Technology, Haifa 32000, Israel
[5] Space Telescope Science Institute, 3700 San Martin Drive, Baltimore, MD 21218, USA
[6] KIPAC/SLAC, 2575 Sand Hill Road M/S 29, Menlo Park, Ca 94025, USA

Abstract. One of the main problems in modeling the ionised outflows in Active Galactic Nuclei is the unknown distance of the outflowing wind to the central source. Only if the density is known this distance can be determined through the ionisation parameter. Here we study density diagnostics based upon O v transitions. O v is known to have metastable levels that are density dependent. We study the population of those levels under photoionisation equilibrium conditions and determine for which parameter range they can have a significant population. We find that resonance line trapping plays an important role in reducing the critical densities above which the metastable population becomes important. We investigate the K-shell absorption lines from these metastable levels. Provided that there is a sufficient population of the metastable levels, the corresponding K-shell absorption lines are detectable and are well separated from the main absorption line originating from the ground state. We then present the Chandra LETGS spectrum of the Seyfert 1 galaxy Mrk 279 that may show for the first time the presence of these metastable level absorption lines. A firm identification is not yet possible due to both uncertainties in the observed wavelength of the strongest line as well as uncertainties in the predicted wavelength. If the line is indeed due to absorption from O v, then we deduce a distance to the central source of one light week to a few light months, depending upon the importance of additional heating processes.

Key words. galaxies: individual: Mrk 279 – galaxies: Seyfert – galaxies: quasars: absorption lines – X-rays: galaxies

1. Introduction

Active Galactic Nuclei (AGN) have X-ray spectra that are dominated by nonthermal emission from the immediate surroundings of a supermassive black hole. Seyfert galaxies constitute the lower luminosity class of AGN. In a significant fraction of all Seyfert galaxies the spectral signatures of the so-called warm absorber are visible (e.g., Reynolds 1997; George et al. 1998). This warm absorber is very likely a photoionised outflow from the accretion disk, with strong UV (for example Crenshaw et al. 1999) and X-ray absorption lines (Kaastra et al. 2000). X-ray observations with high sensitivity show the presence of absorption lines with a broad range of ionisation parameter $\xi = L/nr^2$, where L is the 1–1000 Ryd luminosity, n the density and r the distance to the central source. A good example of this broad range in ionisation parameter is the XMM-Newton Reflection Grating Spectrometer (RGS) spectrum of NGC 5548, which shows the presence of K-shell absorption

lines from all oxygen ions between O III–O VIII (Steenbrugge et al. 2003).

One of the main problems in modeling this outflow is that its distance r from the nucleus is hard to measure. Photoionisation modeling only yields the product nr^2, as well as the column density nd with d the thickness of the absorbing layer in the line of sight. Lacking a density, both the thickness d and the distance r are essentially unknown. Gabel et al. (2003) detected UV absorption lines from the metastable 2s 2p ^{3}P triplet in C III around 1175 Å in the highest velocity outflow component in NGC 3783. These measurements indicate a relatively high density of order 10^{15} m^{-3} corresponding to an upper limit of the distance to the nucleus of 0.3 pc. However these density estimates are somewhat uncertain due to the contamination of the C III resonance line at 977 Å with Galactic absorption in that source. Behar et al. 2003 pointed out that the 2s 2p triplet of C III can in fact be populated at low densities. Only one fine-structure level in the triplet requires high densities (see, e.g., Fig. 1 in Bhatia & Kastner 1993). Indeed

updated calculations by Gabel et al. (2004a) show a lower density of 3×10^{10} m^{-3} and a distance of 25 pc.

Other constraints on density hence distance may be derived from reverberation studies of the warm absorber in response to continuum variations, by measuring the recombination time scale. Long grating observations of NGC 3783 with XMM-Newton (Behar et al. 2003) and with Chandra (Netzer et al. 2003) have allowed for attempts to study the response of the absorber to the ionising continuum through reverberation. However, since no response was detected these could provide only lower limits (of the order of 0.5 pc) to the distance of the absorber from the central source. Reeves et al. (2004) did claim to see variability in the Fe-K absorption of that source, albeit with CCD spectra. They deduce an upper limit to the distance of the absorber to the central source of 0.02 pc.
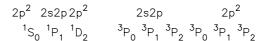
In stellar coronae, with collisional ionisation equilibrium, several X-ray emission lines are density-dependent, for example the forbidden and intercombination lines of the O VII triplet. As these lines have low oscillator strengths, it is impossible to observe them in absorption. In some isoelectronic sequences, close above the ground state of the ion there exist metastable levels that can have a significant population. A well known example is the Be-sequence, where the C III line at 1909 Å is often used as a density diagnostic in plasmas. Another ion in this iso-electronic sequence is O V, where the metastable $1s^2 2s\,2p\ ^3P$ level is only 10 eV above the ground state $1s^2 2s^2\ ^1S_0$. The $J = 0$ term of this triplet cannot decay radiatively to the ground state, leading to a significant population of this level at all densities. K-shell absorption from the ground state of this ion (at 22.3 Å) has been observed in AGN (NGC 5548, Steenbrugge et al. 2003, 2004; NGC 4051, Ogle et al. 2004); and recently Mrk 279 (Costantini et al. 2004). In this last source the spectrum indicates the possible presence of absorption from the metastable level of O V. The critical density for the population of this metastable level is around 10^{16} m^{-3}, a relevant density for AGN outflows. The presence or absence of K-shell absorption lines from the metastable level of O V then is an important density diagnostic, which can serve to constrain distance and geometry of the outflow.

In principle transitions from the metastable level of O V can also be studied using the UV absorption lines from the $2s\,2p$ triplet to $2p^2$ triplet near 760 Å. Pettini & Boksenberg (1986) identified these lines in IUE spectra of the BAL quasar PG 0946+301. However, in HST data of the same object no evidence for these lines was found (Arav et al. 1999). But in yet another BAL quasar (QSO B0226-1024) Korista et al. (1992) found possible evidence for the presence of these lines, implying densities of the order of 10^{17} m^{-3}. However, due to Galactic absorption such an analysis can only be done for bright, highly redshifted quasars. For nearby Seyfert galaxies K-shell X-ray absorption lines are the ideal tool to study densities.

In this paper we study the expected population of the metastable level of O V under photoionised conditions, as well as the wavelengths and oscillator strengths of the corresponding K-shell absorption lines. We then present a possible detection of absorption from O V* levels in the Chandra LETGS spectrum of Mrk 279.

Table 1. Energy levels of O V. Energies are taken from Wiese et al. (1996). Levels 2–4 are the metastable levels discussed in this paper.

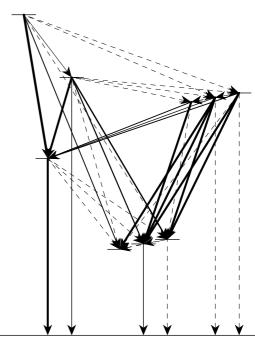| Level	Configuration	J	Energy (eV)
1	$2s^2\ ^1S$	0	0
2	$2s\,2p\ ^3P$	0	10.16
3		1	10.18
4		2	10.21
5	$2s\,2p\ ^1P$	1	19.69
6	$2p^2\ ^3P$	0	26.47
7		1	26.49
8		2	26.52
9	$2p^2\ ^1D$	2	28.73
10	$2p^2\ ^1S$	0	35.70

Fig. 1. Energy level diagram of O V. Only the $n = 2$ levels are shown. The energy differences within the ^3P triplets have been exaggerated for clarity. Solid lines: transitions with transition probabilities larger than 1 s^{-1}; the line thickness is proportional to the logarithm of the transition probability. Dashed lines: transitions with transition probabilities less than 1 s^{-1}.

2. Level populations

2.1. Transition rates

We made a model for the population of all 10 levels with principal quantum number $n = 2$. These levels are listed in Table 1. The energy-level diagram is shown in Fig. 1. We omit the $n > 2$ levels from our calculation, as the lowest of these levels has an energy of 67.82 eV. This is too high as compared to the typical temperatures of a few eV for which O V is formed under photoionised conditions.

The population levels n_i were solved using the equation

$$R_{ij}n_j = b_i, \tag{1}$$

where we sum over j and R_{ij} is the total transition rate matrix from level j to level i, and b_i represents source/loss terms like ionisation from O IV to O V or recombination from O VI to O V. Other loss terms like ionisation or recombination of O V itself can be accomodated in R_{ij}, as these processes are proportional to the O V density.

Radiative transition rates between the levels of Table 1 were taken from the compilation of Wiese et al. (1996).

We took the excitation rates from Safranova et al. (1995) for the following transitions: $2s^2$–$2s\,2p$ and $2s\,2p$–$2p^2$. The remaining rates were taken from Kato et al. (1990). Kato et al. give only the total rates for the following transitions involving a singlet and a triplet: $2s^2$–$2p^2\,^3P$, $2s\,2p\,^3P$–$2s\,2p\,^1P$, $2p^2\,^3P$–$2p^2\,^1D$ and $2p^2\,^3P$–$2p^2\,^1S$. Lacking more information, we therefore subdivided these rates according to the statistical weights of the triplets involved. This is also found to be valid for the distorted wave calculations of Zhang & Sampson (1992), which explicitly give multiplet-resolved rates. There is a caveat, however. As noted by Safranova et al. (1995) in the forbidden transitions ($J' - J = 0$–$0, 0$–$2, 2$–0), only the exchange contribution to the collision strength is important, and the direct part is zero. The $^3P_0$–$^1D_2$, $^3P_0$–$^1S_0$ and $^3P_2$–$^1S_0$ transitions of the above mentioned configurations are forbidden and would suffer from this effect. As however in most astrophysical situations the occupation of the $2p^2$ levels is low, and these levels have strong radiative transitions to lower levels, the errors made by our approximation are not too serious.

We added the proton excitation rates within the $2s\,2p$ and $2p^2\,^3P$ triplets from Doyle et al. (1980).

We also included radiative recombination (O VI to O V and O V to O IV) and collisional ionisation rates (O IV to O V and O V to O VI). We took the total radiative recombination rates from Arnaud & Rothenflug (1985) and assume that the rates towards the $n = 2$ levels, either direct or indirect, are proportional to the statistical weight of these levels. The collisional ionisation rates were also taken from Arnaud & Rothenflug (1985). For ionisation of O IV, we assume that all O IV ions are in the $2s^2 2p\,^2P$ ground state, and that 2s-shell ionisation of O IV results into a $2s\,2p\,^3P$ state of O V with the population of the sublevels distributed according to their statistical weight. Note however that for the parameter range that we consider the collisional ionisation and radiative recombination rates are relatively unimportant.

At low temperatures charge transfer reactions with neutral hydrogen become important. We included the charge transfer recombination rates for recombination of O VI and O V from Rakovic et al. (2001). Similar to the radiative recombination, we assume that the rates towards the $n = 2$ levels, either direct or indirect, are proportional to the statistical weight of these levels.

2.2. Collisional ionisation equilibrium

Using the rates determined in the previous section, we determine equilibrium population levels for a range of densities
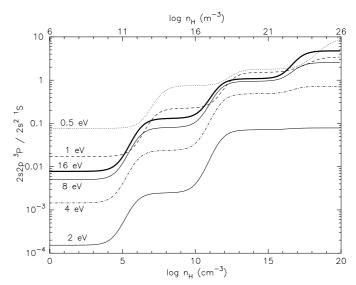

Fig. 2. Population of the $2s\,2p\,^3P$ triplet with respect to the ground state in O V as a function of density and kT (in eV) as labeled. All three sublevels ($J = 0$, $J = 1$ and $J = 2$) have been added.

and temperatures, first under collisional ionisation equilibrium (CIE) conditions. We restrict the temperature range to $kT < 20$ eV; higher temperatures are not expected under photoionised conditions, and moreover they would result in a significant amount of excitation to the $n = 3$ levels, with the corresponding downwards radiative decays.

For this temperature range, the effect of collisional ionisation is negligible, as the electrons have insufficient energy to overcome the 113.896 eV ionisation potential. Radiative recombination affects the population of the $2s\,2p\,^3P$ triplet by no more than 3%. Proton excitation modifies the populations only significantly (more than 3%) for temperatures higher than 10 eV, but even for $kT = 30$ eV the effects are smaller than 11% for all densities.

Charge transfer recombination due to collisions with H I atoms appears to be very important at temperatures below 2 eV. This is mainly due to the large recombination cross section at low temperatures and the high neutral fraction at these low temperatures. Since under CIE conditions the O V fraction is less than 0.001 for temperatures below 9 eV, inclusion of charge transfer recombination is of little practical use under those circumstances, however.

Figure 2 shows the relative occupation P of the $2s\,2p\,^3P$ triplet with respect to the ground state. The enhancement of this ratio at $kT = 0.5$ eV and $kT = 1$ eV is due to the charge transfer recombinations. The sharp increases in P as a function of hydrogen density n_H around densities of a) 10^{12}, b) 10^{17} and c) 10^{22} m^{-3} are due to the following. At a), the collisional coupling of the $2s\,2p\,^3P_2$ level with the $2s\,2p\,^3P_1$ level (either direct or via excitation to the $2p^2\,^3P_1$ level followed by radiative decay) becomes stronger than the radiative decay by a forbidden transition to the ground state. At b), the collisional coupling of the $2s\,2p\,^3P_1$ level with the other triplet levels is stronger than its radiative decay to the ground state. Finally, at c) the ground state depopulates due to strong collisional coupling of the $2s\,2p\,^1P$ level with the $2p^2\,^1D, ^1S$ levels. This causes the
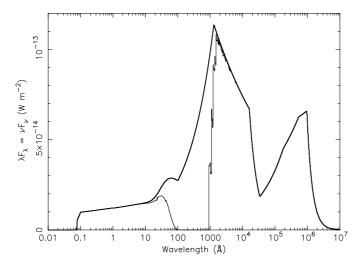
Fig. 3. Spectral energy distribution (thick line) used for our photoionisation calculations. The thin line shows the same spectrum absorbed by a Galactic foreground of cold gas with a hydrogen column density of 1.64×10^{24} m^{-2} and $\sigma_v = 10$ km s^{-1}.

ratio of the triplet with respect to the ground state to increase (the ratio with respect to the sum of all O V levels does not change).

2.3. Photoionisation equilibrium

For photoionised plasmas we use the same approach as before, only the transition matrix R_{ij} and the source term b_i contains more terms. We now include both photo-excitation and stimulated emission between the $n = 2$ levels. As we will use an ionising spectrum with a strong UV component (see below), photo-excitations towards higher levels than $n = 2$ are relatively unimportant. We include photoionisation of O IV from both the 2p and 2s shells. For our ionising spectrum, the photoionisation rate of O IV from the 1s shell is only 2.5% of the 2p rate, and as 1s ionisation of O IV is followed in most cases by an Auger transition, producing O VI, we neglect this process here. We also neglect the similar process of K-shell ionisation of O III followed by an Auger transition, as we assume that the concentration of O III relative to O V may be small and again K-shell photoionisation is rare relative to L-shell photoionisation for our ionising spectrum. However, we included the 5% contribution of 1s photoionisation of O V to the total $n = 2$ photoionisation rate, as this represents a loss term for which we are not interested in the end product.

For the photoionising spectrum we adopt a model based upon the observed Chandra and UV continuum of Mrk 279 (Costantini et al. 2004). This model is similar to the model employed for NGC 5548 by Kaastra et al. (2002). The spectrum contains a strong UV bump (Fig. 3). We normalized it to a 1–1000 Ryd luminosity L of 8.31×10^{37} W, in order to reproduce the observed UV and X-ray continuum of Mrk 279. Note that for this spectral shape the relation between the photoionisation parameters ξ and U is given by $U = Q/4\pi r^2 nc = 0.036\xi$, where Q is the number of hydrogen ionising photons and ξ is expressed in units of 10^{-9} W m. The concentrations of O IV–O VI as well as the temperature $T(\xi)$ as a function of the
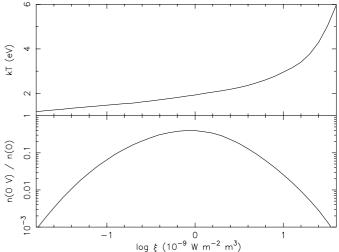

Fig. 4. Temperature (*upper panel*) and O V fraction (*lower panel*) as a function of ionisation parameter ξ. The maximum O V concentration of 40% occurs for $\log \xi = -0.05$, at a temperature $kT = 1.9$ eV (to be compared with 47% at $kT = 21.0$ eV under CIE conditions).
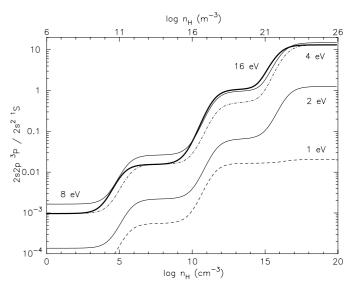

Fig. 5. Population of the 2s 2p ^{3}P triplet with respect to the ground state in O V as a function of density and kT (in eV) as labeled for a photoionised plasma. All three sublevels ($J = 0$, $J = 1$ and $J = 2$) have been added.

ionisation parameter ξ were obtained from a set of runs with Cloudy Version 95.06 (Ferland 2002) for a thin photoionised slab at low density and with solar abundances. In that approximation, $T(\xi)$ and the ion concentrations only depend upon the shape of the ionizing spectrum. Figure 4 shows the O V concentration and $T(\xi)$ relation. We then determined the level populations as a function of n_H and T; inverting $T(\xi)$ yields ξ and using ξ, L and n_H we then know the distance of the absorber to the central source and hence the relevant fluxes for photoionisation and photo-excitation.

We show our results in Fig. 5. At low temperatures ($kT < 1$ eV) the neutral hydrogen fraction is now much smaller than in a collisional equilibrium plasma, resulting in less important effects of charge transfer recombination. For temperatures kT

between 2–4 eV and densities below 10^{20} m^{-3} the results for photoionisation equilibrium (PIE) and CIE are not significantly different. At higher densities photo-excitation of in particular the 2s^2–2s 2p ^{1}P$_1$ resonance line (629.73 Å) is more important than collisional excitation from the ground state to the 2s 2p ^{1}P$_1$ level, causing enhanced higher level populations.

2.4. Resonance line trapping

In Sect. 2.3, our treatment of PIE assumed that O V is located in a photoionised slab with negligible column density. However modeling of the Mrk 279 spectrum shows that O V has a column density of order 10^{20} m^{-2}. For a velocity broadening σ_v of 50 km s^{-1} this implies that the 2s^2–2s2sp ^{1}P$_1$ resonance line has an optical depth of 69 at the line center. As for a broad range of parameter space radiative decay through this emission line is the dominant decay proces of the upper level j, line photons effectively undergo resonance line scattering. The direct escape probability P_{esc} per emitted photon is therefore very small, and this leads effectively to a smaller radiative decay rate $A'_{ij} = P_{esc}A_{ij}$, with A_{ij} the true transition probability. We follow here the approach of Hollenbach & McKee (1979) and Kallman & McCray (1982) in order to approximate P_{esc} for a slab:

$$P_{esc} = \frac{(A_{ij}/A_{tot})}{1. + \tau_0 \sqrt{2\pi \ln(2.13 + \tau_0^2)}}, \qquad (2)$$

where τ_0 is the optical depth at line center, and A_{tot} is the total transition probability from level j to any higher or lower level, including radiative and collisional processes. Resonance line trapping appears to be relevant for the transition between levels 1–5 (629.73 Å) mentioned above, as well as for the 3–6 (761.13 Å), 5–9 (1371.30 Å) and 5–10 (774.52 Å) transitions whenever the 2s 2p configuration has a significant population.

In Fig. 6 we show the results for our calculations including resonance line trapping. It is seen that the critical density at which the 2s 2p triplet level gets a significant population can shift downwards by several orders of magnitude for sufficiently large column densities.

3. X-ray absorption lines

We have calculated wavelengths and oscillator strengths for all transitions between levels with a K-shell vacancy (1s 2s^{2}2p, 1s 2s 2p^2 and 1s2p^3) and the 1s^2 2s^2, 1s^2 2s 2p, 1s^2 2p^2 and 1s^2 2s np levels. We used the code of Cowan (1981) for this purpose.

Table 2 lists the calculated wavelenghts and oscillator strengths f of all lines with $f > 0.001$ and principal quantum number $n < 10$. We determined only total oscillator strengths and average wavelengths of the multiplets, as the current X-ray instrumentation has insufficient resolution to resolve the individual lines of the multiplets.

An important question is the accuracy of the wavelengths. In general these wavelengths have never been measured in the laboratory, with the exception of the resonance transition A2. This wavelength is 22.374 ± 0.003 Å (Schmidt et al. 2004).
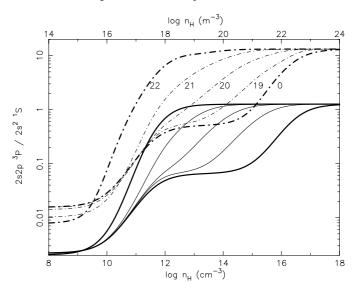

Fig. 6. Population of the 2s 2p ^{3}P triplet with respect to the ground state in O V as a function of density and kT (in eV) in a photoionised plasma. Solid curves are for $kT = 2$ eV, dash-dotted curves for $kT = 4$ eV. Labels indicate log N with N the column density of O V in m^{-2}. All three sublevels ($J = 0$, $J = 1$ and $J = 2$) have been added.

Table 2. Strongest X-ray lines of O V. The values listed apply for the full multiplets (not splitted into sublevels).

Label	Initial state		Final state		f	λ
	Conf.	Term.	Conf.	Term.		(Å)
A2	2s^2	^{1}S	1s 2s^{2}2p	^{1}P	0.649	22.381
A3	2s^2	^{1}S	1s 2s^{2}3p	^{1}P	0.108	19.871
A4	2s^2	^{1}S	1s 2s^{2}4p	^{1}P	0.041	19.258
A5	2s^2	^{1}S	1s 2s^{2}5p	^{1}P	0.020	19.002
A6	2s^2	^{1}S	1s 2s^{2}6p	^{1}P	0.012	18.869
A7	2s^2	^{1}S	1s 2s^{2}7p	^{1}P	0.007	18.791
A8	2s^2	^{1}S	1s 2s^{2}8p	^{1}P	0.005	18.742
A9	2s^2	^{1}S	1s 2s^{2}9p	^{1}P	0.004	18.708
B1	2s 2p	^{3}P	1s 2s 2p^2	(^{3}S)^{3}P	0.328	22.466
B2	2s 2p	^{3}P	1s 2s 2p^2	(^{3}S)^{3}D	0.178	22.431
B3	2s 2p	^{3}P	1s 2s 2p^2	(^{3}S)^{3}S	0.039	22.239
B4	2s 2p	^{3}P	1s 2s 2p^2	(^{1}S)^{3}P	0.014	22.132
C1	2s 2p	^{1}P	1s 2s 2p^2	(^{1}S)^{1}D	0.182	22.558
C2	2s 2p	^{1}P	1s 2s 2p^2	(^{3}S)^{1}P	0.339	22.389
C3	2s 2p	^{1}P	1s 2s 2p^2	(^{1}S)^{1}S	0.040	22.363
D1	2p^2	^{3}P	1s 2s^2 2p	^{3}P	0.005	23.643
D2	2p^2	^{3}P	1s 2p^3	^{3}D	0.173	22.511
D3	2p^2	^{3}P	1s 2p^3	^{3}S	0.151	22.474
D4	2p^2	^{3}P	1s 2p^3	^{3}P	0.105	22.339
E1	2p^2	^{1}D	1s 2s^2 2p	^{1}P	0.006	23.598
E2	2p^2	^{1}D	1s 2p^3	^{1}D	0.328	22.477
E3	2p^2	^{1}D	1s 2p^3	^{3}P	0.002	22.457
E4	2p^2	^{1}D	1s 2p^3	^{1}P	0.112	22.306
F1	2p^2	^{1}S	1s 2s^2 2p	^{1}P	0.002	23.855
F2	2p^2	^{1}S	1s 2p^3	^{1}P	0.438	22.536

The lower levels (1s^2 2ℓ 2ℓ') of these transitions have accurately known energy levels E_i (Wiese et al. 1996). For the upper levels (1s 2ℓ 2ℓ' $n\ell''$) accurate energy levels E_j can be obtained indirectly from Auger electron spectra through the relation $E_j = E_A + I$, with I the ionisation potential of O V, for

Table 3. Core-excited energy levels in O v. Columns (1) and (2): configuration and term; Cols. (3) and (4): calculated energy of the Auger electron E_A for a transition to the $1s^2\,2s$ ^2S (ground) state of O vi where only transition energies to the $1s^2\,2p$ ^2P state are given in the original reference these have been corrected for the energy difference between the ^2S and ^2P state; Col. (5): measured E_A; Col. (6): adopted E_A; Col. (7): adopted energy $E_j = E_A + I$ of the level.

Conf.	Term.	E_A (th) (eV)	E_A (th) (eV)	E_A (exp) (eV)	E_A (eV)	E_j (eV)
$1s\,2s^2\,2p$	^1P	441.16^a	440.55^d	440.5 ± 0.2^f	440.55	554.45 ± 0.20
	^3P	436.63^a	435.96^b	435.9 ± 0.2^f	435.96	549.86 ± 0.20
$1s\,2s^2\,3p$	^1P		507.54^d		507.54	621.44 ± 0.20
$1s\,2s\,2p^2$	^1S	462.10^a	460.83^c	460 ± 2^e	460.83	574.73 ± 0.20
	^1P	461.98^a	460.12^c	460.5 ± 1^e	460.12	574.02 ± 0.20
	^1D	456.74^a	455.35^c	456.3 ± 0.8^e	455.35	569.25 ± 0.20
	^3S	455.06^a	454.17^b	454 ± 1^e	454.17	568.07 ± 0.20
	$(^3S)^3P$	448.76^a	448.70^b	448.6 ± 0.2^f	448.70	562.60 ± 0.20
	$(^1S)^3P$	458.58^a	456.9^e		457.50	571.40 ± 0.60
	^3D	449.74^a	448.68^b	448.5 ± 1^e	448.68	562.58 ± 0.20
	^5P	438.33^a		438.55 ± 0.2^f	438.55	552.45 ± 0.20
$1s\,2p^3$	^1P	473.72^a	471.80^d		471.80	585.70 ± 0.20
	^1D	468.05^a			466.97	580.87 ± 0.60
	^3S	464.91^a			463.83	577.73 ± 0.60
	^3P	469.40^a			468.32	582.22 ± 0.60
	^3D	463.75^a			462.67	576.57 ± 0.60
	^5S	456.27^a		456.4 ± 0.2^f	456.40	570.30 ± 0.20

^{a} Chen (1985).
^{b} Lin et al. (2001).
^{c} Shiu et al. (2001).
^{d} Lin et al. (2002).
^{e} Bruch et al. (1979).
^{f} Bruch et al. (1987).

Table 4. Wavelength comparison of the X-ray lines of O v. Wavelengths are given in Å. The column "Cowan" gives λ from Table 2; "corr." are these calculated wavelengths corrected as described in the text; "Auger" are the wavelengths determined from Auger energies as listed in Table 3; "CC" are the calculations by Chen & Crasemann (1987); "HULLAC" are the wavelengths calculated using the HULLAC code.

Line	Cowan	Corr.	Auger	CC	HULLAC
A2	22.381	22.374	22.362 ± 0.008	22.415	22.372
A3	19.871	19.866	19.951 ± 0.008		19.921
A4	19.258	19.253			19.316
A5	19.002	18.997			19.060
A6	18.869	18.864			18.949
A7	18.791	18.786			18.849
A8	18.742	18.737			18.800
A9	18.708	18.703			18.766
B1	22.466	22.488	22.444 ± 0.008	22.535	22.425
B2	22.431	22.453	22.445 ± 0.008	22.494	22.415
B3	22.239	22.260	22.224 ± 0.008	22.279	22.197
B4	22.132	22.153	22.092 ± 0.024	22.139	22.091
C1	22.558	22.589	22.561 ± 0.008	22.668	22.522
C2	22.389	22.419	22.367 ± 0.008	22.453	22.365
C3	22.363	22.393	22.338 ± 0.008	22.448	22.349
D1	23.643	23.670	23.690 ± 0.009	23.790	23.572
D2	22.511	22.538	22.540 ± 0.024	22.615	22.478
D3	22.474	22.501	22.492 ± 0.024	22.566	22.404
D4	22.339	22.365	22.311 ± 0.024	22.383	22.331
E1	23.598	23.597	23.584 ± 0.009	23.747	23.520
E2	22.477	22.476	22.455 ± 0.024	22.584	22.430
E3	22.457	22.456	22.400 ± 0.024	22.529	22.479
E4	22.306	22.305	22.260 ± 0.008	22.353	22.283
F1	23.855	23.908	23.901 ± 0.009	24.112	23.765
F2	22.536	22.589	22.543 ± 0.008	22.677	22.503

which we take 113.896 eV (Wiese et al. 1996), and E_A the energy of the Auger electron.

E_A has been measured in the laboratory or calculated theoretically; we list the relevant values in Table 3. A comparison of the calculations of the group of K.T. Chung (Lin et al. 2001; Shiu et al. 2001; Lin et al. 2002) with the measurements of Bruch et al. (1979, 1987) shows excellent agreement; the average difference between observed and calculated values is -0.05 ± 0.16 eV; we therefore adopt a nominal uncertainty of 0.20 eV for these calculated energies, equal to the measurement errors in the best measurements. A comparison of the energies calculated by Chen (1985) with the above mentioned calculations by the group of K.T. Chung shows an average difference of 1.08 ± 0.28 eV, with a standard deviation of 0.60 eV for the 9 levels in common. Therefore whenever we use the energies calculated by Chen, we subtract 1.08 eV and assign a nominal accuracy of 0.60 eV.

The adopted energies E_j of Table 3 were combined with the lower level energies E_i of Table 1 in order to calculate the predicted wavelengths of the transitions from Table 2. We list those wavelengths in Table 4. Champeaux et al. (2003) recently deduced the ionisation potential I for O v to be 113.66 ± 0.13 eV, based upon the quantum defect estimated from resonances in the measured photoionisation cross section. If this value is used instead of the value of 113.896 eV given by Wiese et al. (1996), most wavelengths listed in the column "Auger" of Table 4 increase by 0.009 Å.

A comparison of the energies of the $1s^2 2\ell 2\ell'$ levels calculated by us using the Cowan (1981) code with the values of Table 1 (Wiese et al. 1996) shows that our calculated energies are smaller by 0.71 (levels 2–4), 0.91 (level 5), 0.83 (levels 6–8), 0.16 (level 9) and 1.46 eV (level 10), respectively. Correcting all wavelengths where these levels are involved by these differences and also adjusting all K-shell vacancy states by the same number so as to get the laboratory wavelength of the 22.374 Å line correct, yields the column labeled with "corr." in Table 4. The difference in wavelength between both columns can be as large as 0.053 Å, comparable to the energy resolution of Chandra's LETGS. Finally, we list in Table 4 also wavelengths from the paper by Chen & Crasemann (1987) as well as wavelengths presently calculated with the Hebrew University Lawrence Livermore Atomic Code (HULLAC).

In general, the theoretical calculations for the wavelengths differ quite a lot. We illustrate this with the resonance line at 22.374 Å. Calculated values range from 22.362 Å (Auger measurements) to 22.415 Å (Chen & Crasemann); for comparison, Pradhan et al. (2003) give a value of 22.35 Å.

Table 5. Oscillator strengths f, total transition probabilities A_{rad}, Auger decay rates A_{A} and total transition rates A_{tot} of O V. Transition probabilities are in units of 10^{12} s^{-1}.

id	$f^{\,a}$	$f^{\,b}$	$A_{\mathrm{rad}}{}^{a}$	$A_{\mathrm{rad}}{}^{b}$	$A_{\mathrm{A}}{}^{a,c}$	$A_{\mathrm{tot}}{}^{d}$
A2	0.646	0.649	3.05	3.00	87.9	90.9
A3		0.108		0.63	129	129.6
A4		0.041		0.26	129	129.3
A5		0.020		0.13	129	129.1
A6		0.012		0.07	129	129.1
A7		0.007		0.05	129	129.1
A8		0.005		0.03	129	129.0
A9		0.004		0.02	129	129.0
B1	0.326	0.328	4.29	4.34	34.2	38.5
B2	0.171	0.178	1.35	1.41	94.2	95.6
B3	0.039	0.039	1.56	1.56	46.9	48.5
B4	0.014	0.014	0.19	0.19	100	100.2
C1	0.181	0.182	1.41	1.43	213	214.4
C2	0.333	0.339	4.40	4.51	22.9	27.4
C3	0.041	0.040	1.63	1.60	154	155.6
D1	0.007	0.005	0.08	0.06	129	129.1
D2	0.169	0.173	1.32	1.37	131	132.4
D3	0.153	0.151	6.00	5.99	0.0015	6.0
D4	0.102	0.105	1.36	1.42	79.9	81.3
E1	0.009	0.006	3.05	3.00	87.9	90.9
E2	0.330	0.328	4.31	4.35	130	134.4
E3	0.000	0.002	1.36	1.42	79.9	81.3
E4	0.111	0.112	4.36	4.41	76.9	81.3
F1	0.003	0.002	3.05	3.00	87.9	90.9
F2	0.439	0.438	4.36	4.41	76.9	81.3

[a] Chen & Crasemann (1987).
[b] Present work.
[c] For A3–A9 see text.
[d] Using $A_{\mathrm{tot}} = A_{\mathrm{rad}} + A_{\mathrm{A}}$ with A_{rad} from the present work.

There is a good agreement between our calculations for oscillator strengths and transition probabilities and those of Chen & Crasemann (1987), see Table 5. The rms difference between both sets of oscillator strength is 0.003. Also, the total radiative transition probabilities from core-excited levels agree within 2%. It is necessary to take also the Auger transitions into account for estimating the lifetime of the core-excited levels. We use the Auger rates determined by Chen & Crasemann (1987). Their rates are in good agreement with the calculations of Lin et al. (2001, 2002) for the 6 levels in common. These Auger rates are an order of magnitude larger than the radiative transition rates. Thus neglecting Auger rates will affect the estimated line equivalent width for high column densities. There are no Auger rates available for the A4–A9 transitions. Lin et al. (2002) calculate an Auger rate of 1.29×10^{14} s^{-1} for the upper level of transition A3. In their calculations for Be, they find that for higher principal quantum number n the Auger rates do not depend strongly upon n. Therefore we adopt a constant value for A_{A} for transitions A3–A9.
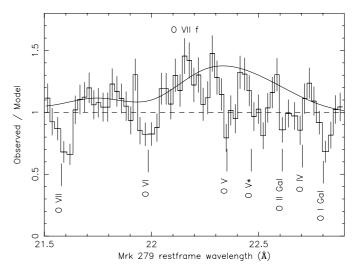

Fig. 7. Chandra LETGS spectrum of Mrk 279 near the oxygen absorption lines. The observed spectrum has been divided by the best fit simple continuum model described in the text (dashed line). The additional broad emission feature is indicated by the curved line. The wavelength scale is for the restframe of Mrk 279 (at $z = 0.0306$). In the line identifications, we have taken into account a small outflow (blueshift) of 300 km s^{-1} with respect to this restframe; this outflow has been measured using simultaneous high-resolution UV spectra. A few Galactic absorption lines are labeled with "Gal".

4. Comparison with the observed spectrum of Mrk 279

4.1. Chandra LETGS observations

Mrk 279 is a moderately distant ($z = 0.0306$) Seyfert 1 galaxy that we observed for 340 ks with the Chandra LETGS. This instrument has a spectral resolution of ~0.05 Å *FWHM*. The full data analysis of the LETGS spectrum of Mrk 279 will be presented elsewhere (Costantini et al. 2004). Here we only summarize the results relevant for the study of the O V absorption lines. The LETGS spectrum was fit by a simple power law plus modified blackbody with Galactic absorption. This smooth continuum spectrum produces an excellent fit to the data except for the few regions where Mrk 279 has absorption lines. The column densities in Mrk 279 are several times smaller than in other well-studied AGN, and therefore most absorption lines and edges are very weak except for the lines from the most abundant metal, which is oxygen. These lines are predominantly found in the 18–24 Å band.

Our continuum fit is excellent everywhere except for the region near the K-shell transitions of oxygen (Fig. 7). Here a broad emission feature with a peak amplitude of about 30% of the continuum is visible. Similar broad X-ray emission lines have been seen before in other AGN (Kaastra et al. 2002; Steenbrugge et al. 2004), and may have asymmetric line profiles. This broad line is due to the O VII triplet from the broad line region. The presence of this broad feature makes the estimate of the underlying continuum for the narrow absorption lines less certain. We estimated the broad line profile by drawing a spline through the spectral regions that are known to be line-free.

Table 6. Observed absorption lines in Mrk 279, due to or related to O V. The observed wavelength λ is given with two error bars: the first is the statistical uncertainty, the second the systematic due to the wavelength calibration uncertainty of the LETGS. For lines with wavelength fixed, the observed equivalent width (*EW*) is merely the formal upper limit. The line around 22.50 Å is either fitted by a single line (22.540 Å) or alternatively by two lines (22.501 and 22.548 Å).

λ (Å)	*EW* (mÅ)	Identification
$22.377 \pm 0.009 \pm 0.008$	18 ± 6	A2
19.957 (fixed)	2 ± 8	A3
19.325 (fixed)	6 ± 6	A4
$22.540 \pm 0.009 \pm 0.010$	20 ± 5	B1+B2?; see text
$22.501 \pm 0.016 \pm 0.010$	10 ± 6	B1+B2?; see text
$22.548 \pm 0.010 \pm 0.010$	18 ± 6	?; see text
$22.269 \pm 0.015 \pm 0.006$	10 ± 6	B3? ; see text

From a detailed study of the O VI UV and X-ray lines (Gabel et al. 2004b; Costantini et al. 2004) we find that the dominant absorber has an outflow velocity of 300 km s^{-1} and a line profile that can be approximated to first order by a Gaussian with $\sigma_v = 50$ km s^{-1}.

4.2. Observed O V lines

We clearly see the absorption at 22.37 Å, which we identify as the $1s^2\,2s^2$–$1s\,2s^2\,2p\ ^1P_1$ transition of O V (Fig. 7). Its measured wavelength in the rest frame of Mrk 279, corrected for the 300 km s^{-1} outflow velocity, is 22.377 ± 0.009 Å, in excellent agreement with the laboratory wavelength of 22.374 Å mentioned before (Schmidt et al. 2004). The quoted error bar is only the statistical error; we estimate the systematic uncertainty (due to calibration uncertainties in the HRC-S detector) to be 0.008 Å.

We find no clear evidence for transition A3. Upper limits to its equivalent width depend upon the adopted wavelength. In another Seyfert 1 galaxy with a strong A2 line we find evidence for a 2σ detection of transition A3 at a laboratory wavelength of 19.957 ± 0.015 Å, right within the wavelength range indicated in Table 4. We adopt this wavelength for transition A3 and use it to measure the limits to the line equivalent width (Table 6). We also do not detect line A4. We take here the wavelength as calculated with the HULLAC code to estimate the equivalent width. Using the velocity broadening σ_v of 50 km s^{-1} and the equivalent widths of lines A2, A3 and A4, we find a column density of $10^{20.16\pm0.42}$ m^{-2} for O V in its ground state. The large uncertainty is mainly due to the strong saturation of the A2 line, which has an optical depth of 3.7 at its line center.

Most absorption lines in the spectral band displayed in Fig. 7 can be easily identified by Galactic absorption lines or absorption lines due to the warm absorber. Only the feature around 22.50 Å has no obvious identification with absorption from the ground state of any abundant ion, either in the warm absorber or the Galactic foreground. When fitted by a single line, its laboratory wavelength, corrected for the
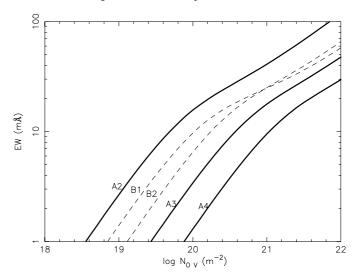

Fig. 8. Curve of growth for the most important K-shell absorption lines of O V, for a Gaussian velocity broadening σ_v of 50 km s^{-1}.

300 km s^{-1} outflow, is 22.540 ± 0.009 Å. A marginally better fit ($\Delta\chi^2 = -3.6$ for two additional degrees of freedom) is obtained for a double, blended line, with laboratory wavelengths of 22.501 ± 0.016 Å and 22.548 ± 0.010 Å, respectively (see Table 6). Again, quoted errors are statistical only; the systematic uncertainty is 0.010 Å and is not correlated with the systematic uncertainty in the main 22.374 Å line.

We suggest that in the case of a double blended line, the 22.501 Å component of the blend may be due to a combination of the B1 and B2 lines of O V, which have a wavelength in the 22.47–22.53 Å range. For the single line solution (22.540 Å) this is somewhat less likely. We note that the added statistical and systematic uncertainty of the measurement of the line centroid is in the 0.02–0.03 Å range. The problem with a firm identification lies of course in both the uncertainty in the theoretical wavelength as well as in the measured wavelength.

If our identification is true, we can deduce the column density of O V in its $2s\,2p\ ^3P$ triplet state. From the curve of growth (see Fig. 8) and an equivalent width of 10 ± 6 mÅ, we find a column of $10^{19.82\pm0.44}$ m^{-2}. This combined with the column density of O V in its ground state yields a value for the population of the $2s\,2p\ ^3P$ triplet state relative to the ground state of 0.5, with rms error bounds of a factor of 4 (i.e., the relative population is between 0.125 and 2). From the column density of the $2s\,2p\ ^3P$ triplet state we predict that line B3 should have an equivalent width of 1 mÅ with an upper limit of 3 mÅ. The feature at 22.269 Å (see Table 6) could be marginally consistent with this.

Table 7 list the densities derived from the population ratio for a few temperatures.

From our photoionisation equilibrium calculations, it follows that O V has its maximum concentration for $kT = 2$ eV (see Fig. 4). This yields a lower limit to the density of 2.5×10^{18} m^{-3}. $kT = 2$ eV corresponds to $\xi = 0.9 \times 10^{-9}$ W m^{-2} m^3, which then leads to an upper limit to the distance r of 2×10^{14} m or one light week. This would place the O V absorber close to the inner broad line region. Although not completely impossible, such a small radius is not very plausible, because Balmer

Table 7. Densities (in m^{-3}) for 2s 2p triplet to ground ratio's of 0.125, 0.5 and 2, for a total O V column density of 1.5×10^{20} m^{-2}.

kT (eV)	0.125	0.5	2
2	2.5×10^{18}	3×10^{19}	∞
4	10^{17}	10^{18}	1.5×10^{19}
6	5×10^{16}	4×10^{17}	10^{19}

line time-delay measurements suggest a broad emission line region size of 6–17 light days for Mrk 279 (Scott et al. 2004, and references therein), and UV spectra show that the broad lines are covered by the warm absorber.

The temperature may be higher than 2 eV, however, if additional heating processes occur in the absorbing region. Cloudy (Ferland 2002) allows for the inclusion of additional heat sources. A temperature of 6 eV is reached for $\xi = 0.7 \times 10^{-9}$ W m^{-2} m^3, with an additional heating rate of 1.0×10^{-7} n_{14}^2 W m^{-3}, where n_{14} the density in units of 10^{14} m^{-3}. In this case the additional heat source dominates the total heating rate. This is also the case for all temperatures above 3 eV, where the additional heating contributes more than 80% to the total heating rate. We find for $kT = 6$ eV a lower limit to the density of 5×10^{16} m^{-3}, corresponding to an upper limit to the distance of 1.5×10^{15} m or 59 light days. This would place the absorber outside the broad line region.

Is there a possible heating process that can produce the additional heat? For the lower limit to the density of 5×10^{16} m^{-3}, the required heating rate Q is 0.025 W m^{-3}. One possibility would be classical heat conduction from a neighbouring hot region. Using a hydrogen column density of 8×10^{23} m^{-2} (corresponding to a typical O V column of 1.5×10^{20} m^{-2}) and the lower limit of 5×10^{16} m^{-3} for the density, we find an upper limit to the size d of the absorber of 1.6×10^7 m. For a heat conductivity κ of 10^{-10} $T_K^{5/2}$ W K^{-1} m^{-1} with T_K the temperature in K, and putting the heating rate Q due to conduction equal to $\kappa T / d^2$, we find that we need a temperature of 300 eV for the hot gas surrounding the absorbing medium. Hotter gas in photoionisation equilibrium coexisting with colder gas is indeed known to be possible. As the geometry of the absorbing regions is still not fully understood, we leave this scenario as an interesting possibility.

In our above analysis, we assumed that as far as O V is concerned the physical conditions in the absorber are such that O V has its maximum relative concentration. It is of course also possible to have a hotter absorber with a smaller concentration of O V. For instance, without invoking an additional heat source we find that $kT = 4$ eV if ξ is 20 times larger than we used before, and correspondingly the O V/O ratio is 100 times smaller. In that case most of the oxygen should be in the form of O VII. Our column densities for O VI and O VII (see Costantini et al. 2004) are not inconsistent with such a scenario. In this case, we avoid the additional heating problem, but of course we still require a high density $n > 10^{17}$ m^{-3} in order to get the high metastable population fraction. In this case however the distance to the central source is only 2×10^{14} m or 8 light days.

We do not expect blending due to lines from higher levels to be important for all temperatures below 4 eV (the line series labeled with C–F of Table 2). This is because for those temperatures the population of these higher levels is small.

Finally, if the metastable level has a significant population, also the UV absorption lines from this level should be detectable in principle. Unfortunately the strong, allowed UV absorption lines from the metastable level are in the unobserved part of the UV spectrum (near 760 Å). If the density would be very high such that also the 2s 2p $^1P_1$ level gets a high population, then the strongest UV absorption line should be the transition between levels 5–9 of Table 1 at 1371.30 Å. Simultaneous HST observations of Mrk 279 (Gabel et al. 2004b) yield an upper limit to the column density for level 5 deduced from the non-detection of this line of 5×10^{16} m^{-2}. Combined with the allowed range for the ground state column density ($10^{19.82 \pm 0.44}$ m^{-2} as quoted before) this leads to an upper limit of 10^{-3} for the population of level 5 with respect to the ground. The corresponding upper limit to the density of 5×10^{17} m^{-3} is consistent with the lower limits derived from the X-ray transition from the metastable level. It should be noted, however, that the X-ray derived density constraints depend on several modeling and observational factors, as is evident from our present discussion.

5. Conclusions

We have investigated in this paper the population of the metastable level of O V under photoionised conditions. For sufficiently high densities and a temperature of just a few eV the metastable levels can have a significant population. The relevant critical densities also depend strongly upon the column density, due to resonance line trapping. The population of higher levels than the 2s 2p ^3P triplet is always relatively small. If the metastable level has a significant population, then we should observe K-shell absorption lines from these levels. The wavelengths of these lines are not very accurately known, however. This makes the identification of these lines in the X-ray spectrum of the Seyfert 1 galaxy Mrk 279 somewhat uncertain. If present, however, then the observed equivalent widths imply densities of order 10^{17} m^{-3} or more, corresponding to a distance to the central source of the order of a light month.

References

Arav, N., Korista, K. T., de Kool, M., Junkkarinen, V. T., & Begelman, M. C. 1999, ApJ, 516, 27
Arnaud, M., & Rothenflug, R. 1985, A&AS, 60, 425
Behar, E., Rasmussen, A. P., Blustin, A. J., et al. 2003, ApJ, 598, 232
Bhatia, A. K., & Kastner, S. O. 1993, ApJ, 408, 744
Bruch, R., Schneider, D., Schwarz, W. H. E., et al. 1979, Phys. Rev. A, 19, 587

Bruch, R., Stolterfoht, N., Datz, S., et al. 1987, Phys. Rev. A, 35, 4114

Champeaux, J.-P., Bizau, J.-M., Cubaynes, D., et al. 2003, ApJS, 148, 583

Chen, M. H. 1985, Phys. Rev. A, 31, 1449

Chen, M. H., & Crasemann, B. 1987, ADNDT, 37, 419

Costantini, E., Kaastra, J. S., Arav, N., et al. 2004, in preparation

Cowan, R. D. 1981, The theory of atomic structure and spectra (Berkeley: Univ. of California Press)

Crenshaw, D. M., Kraemer, S. B., Boggess, A., et al. 1999, ApJ, 516, 750

Doyle, J. G., Kingston, A. E., & Reid, R. H. G. 1980, A&A, 90, 97

Ferland, G. J. 2002, Hazy, a brief introduction to Cloudy 96, Univ. Kentucky Phys. and Astron. Dept. internal report

Gabel, J. R., Crenshaw, D. M., Kraemer, S. B., et al. 2003, ApJ, 583, 178

Gabel, J. R., Kraemer, S. B., & Crenshaw, D. M. 2004a, in AGN physics with the SDSS, ASP Conf. Ser., 311, 239

Gabel, J. R., et al. 2004b, in preparation

George, I. M., Turner, T. J., Netzer, H., et al. 1998, ApJS, 114, 73

Hollenbach, D., & McKee, C. F. 1979, ApJS, 41, 555

Kaastra, J. S., Mewe, R., Liedahl, D. A., Komossa, S., & Brinkman, A. C. 2000, A&A, 354, L83

Kaastra, J. S., Steenbrugge, K. C., Raassen, A. J. J., et al. 2002, A&A, 386, 427

Kallman, T. R., & McCray, R. 1982, ApJS, 50, 263

Kato, T., Lang, J., & Berrington, K. E. 1990, ADNDT, 44, 133

Korista, K., Weymann, R. J., Morris, S. L., et al. 1992, ApJ, 401, 529

Lin, S.-H., Hsue, C.-S., & Chung, K. T. 2001a, Phys. Rev. A, 64, 12709

Lin, S.-H., Hsue, C.-S., & Chung, K. T. 2001b, Phys. Rev. A, 65, 32706

Netzer, H., Kaspi, S., Behar, E., et al. 2003, ApJ, 599, 933

Ogle, P. M., Mason, K. O., Page, M. J., et al. 2004, ApJ, 606, 151

Pettini, M., & Boksenberg, A. 1986, in New Insights in Astrophysics, Eight Years of UV Astronomy with IUE, ESA-SP 263, 627

Pradhan, A. K., Chen, G. X., Delahaye, F., Nahar, S. N., & Oelgoetz, J. 2003, MNRAS, 341, 1268

Rakovic, M., Wang, J. G., Schultz, D. R., & Stancil, P. C. 2001, ORNL/UGA Charge Transfer Database for Astrophysics, http://www-cfadc.phy.ornl.gov/astro/ps/data/

Reeves, J. N., Nandra, K., George, I. M., et al. 2004, ApJ, 602, 648

Reynolds, C. S. 1997, MNRAS, 286, 513

Safranova, U. I., Shlyaptseva, A. S., Kato, T., Masai, K., & Vainshtein, L. A. 1995, ADNDT, 60, 1

Schmidt, M., Beiersdorfer, P., Chen, H., et al. 2004, ApJ, 604, 562

Scott, J. E., Kriss, G. A., Lee, J. C., et al. 2004, ApJS, 152, 1

Shiu, W. C., Hsue, C.-S., & Chung, K. T. 2001, Phys. Rev. A, 64, 22714

Steenbrugge, K. C., Kaastra, J. S., de Vries, C. P., & Edelson, R. 2003, A&A, 402, 477

Steenbrugge, K. C., Kaastra, J. S., Crenshaw, D. M., et al. 2004, A&A, submitted

Wiese, W. L., Fuhr, J. R., & Deters, T. M. 1996, J. Phys. Chem. Ref. Data, Monograph 7

Zhang, H. L., & Sampson, D. H. 1992, ADNDT, 52, 143